Int. J. Electrochem. Sci., 17 **(2022)** Article Number: 220932, doi: 10.20964/2022.09.30

International Journal of
ELECTROCHEMICAL
SCIENCE
www.electrochemsci.org

Simulation and Experimental Analyses of Multi-field Coupling in Electrochemical Machining

Xiaochen Jiang[1,*], *Dan Li*[2], *Zhixiang Xu*[1]

[1] School of Mechanical and Electrical Engineering, Shandong Jianzhu University, Jinan, China, 250101
[2] Hydrology Center of Shandong Province, Jinan, China, 250002
[*]E-mail: jiangxiaochen20@sdjzu.edu.cn

Received: 25 May 2022 / *Accepted:* 29 June 2022 / *Published:* 7 August 2022

Electrochemical machining (ECM) has great advantages in processing and manufacturing and is now used widely in the fields of aviation, aerospace, weapons, and medicine, among others. However, in the actual ECM process, the machining gap between the tool cathode and the workpiece affects the machining accuracy to a certain extent, and reducing the machining gap is one of the main ways to improve the accuracy of ECM. For a better understanding of the coupling among the multiple physical fields in ECM and the influence of the machining gap, this paper simulates and analyzes multi-field coupling in direct-current ECM (DC-ECM), pulsed ECM (PECM), and vibration-assisted PECM (VPECM) for machining gaps of 0.1 mm and 0.01 mm. Based on finite-element multi-field-coupling models of DC-ECM, PECM, and VPECM, how the electric field, flow field, bubble rate, and Joule heat distribution change in the small machining gap is analyzed. The results show that the cathode vibration in VPECM improves significantly the ability of the electrolyte to discharge products. Compared with DC-ECM and PECM, VPECM offers stable machining in a smaller machining gap. To observe the process of product transportation, a high-speed camera was used to see inside the VPECM machining gap.

Keywords: Electrochemical machining; Machining gap; Multi-field coupling; Vibration

1. INTRODUCTION

Higher industrial standards and the emergence of many complex precision parts pose great challenges for electrochemical machining (ECM) technology. Because ECM is a processing method that involves removing workpiece materials in the form of metal ions (which from analyzing its processing principle is generally at a level below the nanometer one), it can in principle achieve micrometer or even nanometer precision [1]. However, in the actual ECM process, the machining gap (MG) between the tool cathode and the workpiece affects the machining accuracy to a certain extent, and reducing the MG is one of the main ways to improve the accuracy of ECM [2]. The MG is affected by many machining parameters, such as electrolyte concentration, electrolyte temperature, flow field, machining voltage, current density, and feed rate, which is why precision ECM for improved machining accuracy has always been a research focus in ECM technology; much research has been done in this regard, and much progress has been made [3–5].

Compared with the situation with a larger MG, the difference in current density on the uneven machined surface of the workpiece is more obvious with a smaller MG, and the dissolution rate in the large allowance area is significantly higher than that in other areas. Reducing the MG is effective for improving the machining replication and repetition accuracies, but making the MG too small reduces the overcurrent area of electrolyte flowing through it. The electrolyte can then not remove electrochemical reaction products in time, thereby leading to the continuous accumulation of products in the MG [6], and these accumulated products short-circuit the contact between anode and cathode, thereby burning the workpiece and damaging the machining tool. Therefore, the core problem in improving the machining accuracy of ECM is achieving a small but stable MG, for which there are two main methods, i.e., pulsed ECM (PECM) and vibration-assisted PECM (VPECM) [7].

Unlike the traditional direct-current ECM (DC-ECM), PECM uses pulsed electricity, which alleviates the accumulation rate of products in the MG to a certain extent [8]. In VPECM, the MG changes periodically, with material removal beginning when the MG is at its smallest; vibrating the tool electrode disturbs the electrolyte and alleviates greatly the adhesion of insoluble products on the workpiece surface. Many scholars have researched PECM and VPECM. Brusilovski et al. [9] studied the influences of many machining parameters on the MG in PECM. Damme [10] established a two-dimensional model of high-speed PECM. Hewidy et al. [11] analyzed the influence of vibration on ECM by establishing a mathematical model, and they verified that vibration can improve the machining accuracy of ECM. Bhattacharyya et al. [12,13] explored the optimal processing parameters and proposed that with a small MG, removal is better with a low vibration frequency than with one of the order of kilohertz. Through comparative tests, Ruszaj et al. [14] showed that (i) VPECM offers better surface quality than does PECM and (ii) the complex engraving of VPECM with abrasive offers better surface quality. Wang et al. [15] suggested that VPECM is more suitable for high-precision machining of narrow slits through comparative experiments.

For a better understanding of the coupling among the multiple physical fields in ECM and the influence of the MG on the distribution of machining products, this paper simulates and analyzes multi-field coupling in DC-ECM, PECM, and VPECM for MGs of 0.1 mm and 0.01 mm. Based on finite-element multi-field-coupling models of DC-ECM, PECM, and VPECM, how the electric field, flow field, bubble rate, and Joule heat distribution change in the small MG is analyzed. To observe the process of product transportation, a high-speed camera was used to see inside the MG in VPECM.

2. PROCESSING PRINCIPLES OF DC-ECM, PECM, AND VPECM

DC-ECM, PECM, and VPECM are the three most typical ECM modes. During DC-ECM, the cathode and workpiece are connected to the negative and positive pole of the power supply, respectively, so that the workpiece maintains a stable positive pressure relative to the cathode. DC-ECM is a continuous machining process that leads to a high proportion of products in the MG; in the small MG, the ability of the electrolyte to remove products decreases because of the decreased electrolyte flow rate, and in the meantime all kinds of products accumulate rapidly. PECM uses a periodic on–off pulsed voltage to replace the stable voltage in DC-ECM; using a pulsed voltage is effective for reducing the generation of products, and at the same time the pressure wave caused by intermittent hydrogen evolution in the gap disturbs the electrolyte and makes it difficult for products to accumulate. VPECM makes the MG expand and narrow alternately and strengthens the renewal of electrolyte; the cathode is powered on for machining when it approaches the machined part of the workpiece and is powered off when it is far away, and anodic dissolution always occurs when the gap becomes smaller. The different types of ECM are shown schematically in Figure 1.

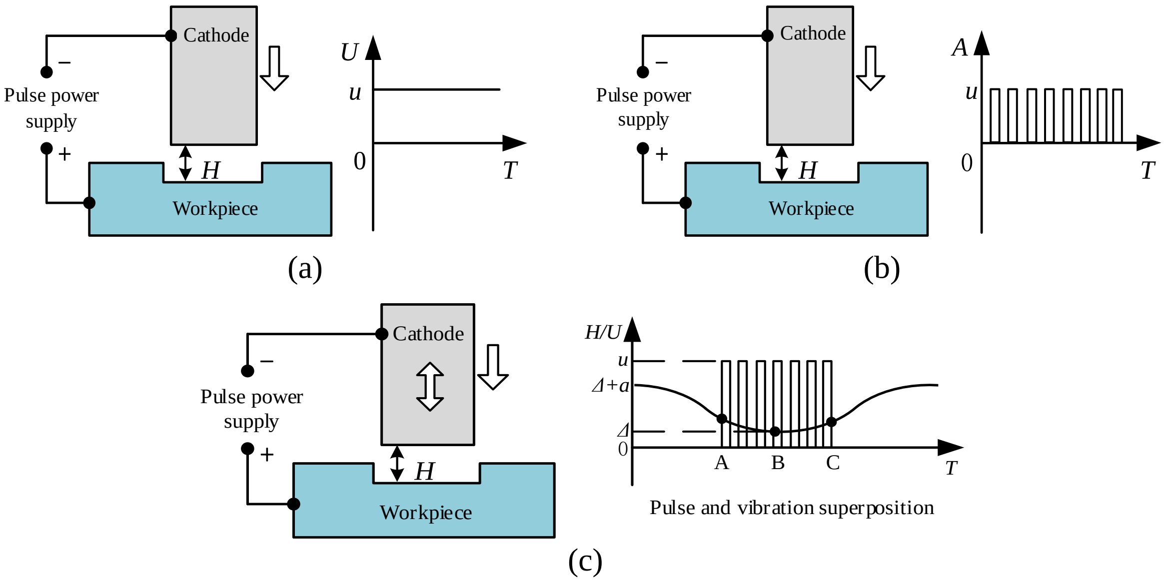

Figure 1. Schematics of different types of electrochemical machining (ECM): (a) direct-current ECM (DC-ECM); (b) pulsed ECM (PECM); (c) vibration-assisted PECM (VPECM)

3. MULTI-FIELD-COUPLING MODEL OF ECM

To explore the differences among the different types of ECM, the electric-field, fluid heat-transfer, and moving-grid modules in the COMSOL Multiphysics simulation software were used for the multi-field physical coupling simulation analysis.

The basic simulation model of ECM is shown in Figure 2, with which the MGs of 0.1 mm and 0.01 mm were simulated and analyzed. The electrolyte flowed in from the inlet (boundary 10) and out from the outlet (boundary 4). The distance between the inlet and the outlet was 30 mm, and the length of the anode (workpiece) and cathode was 20 mm. During the simulations of DC-ECM and PECM, the MG between the cathode and workpiece was fixed at either 0.1 mm or 0.01 mm. During the simulation of VPECM, the motion track of the cathode was simplified to harmonic motion with an amplitude of 0.3 mm; with the reciprocating motion of the cathode, the MG between the workpiece and cathode was 0.1 mm or 0.01 mm at minimum and 0.7 mm or 0.61 mm at maximum.

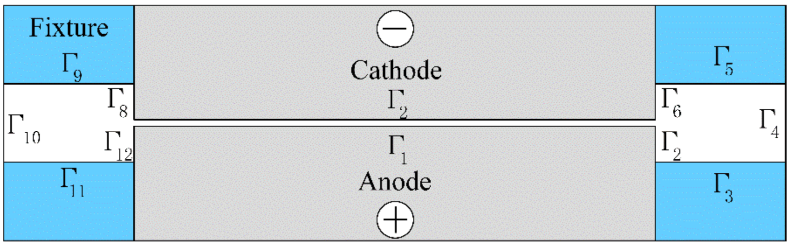

Figure 2. Basic simulation model of ECM

To simplify the model and facilitate simulation analysis, the following relevant assumptions were made: (i) the heat for increasing the electrolyte temperature in the MG is Joule heat, ignoring the heat of electrochemical reaction; (ii) the electrolyte is an incompressible Newtonian fluid; (iii) the surfaces of the workpiece and cathode are equipotential surfaces with different potentials.

3.1 Governing equations and boundary conditions in simulations

In the simulations, the electric field in the MG was governed by the Laplace equation [16], i.e.,

$$\nabla^2\varphi = 0. \tag{1}$$

Equipotential surfaces with different potentials formed on the surfaces of the workpiece and cathode, while the other boundaries were either closed or approximately closed, so the boundary conditions of ECM in the electric-field simulation were set as

$$\varphi|\Gamma_{1,2,12} = U \text{ (anode)}, \tag{2}$$

$$\varphi|\Gamma_{6,7,8} = 0 \text{ (cathode)}, \tag{3}$$

$$\left.\frac{\partial\varphi}{\partial n}\right|\Gamma_{3,4,5,9,10,11} = 0. \tag{4}$$

The bubble rate of gas in two-phase gas–liquid flow is

$$\beta = \frac{Q_1}{Q} = \frac{Q_1}{Q_1+Q_2}, \tag{5}$$

where Q [m^3] is the total volume of gas and liquid, Q_1 [m^3] is the gas volume, and Q_2 [m^3] is the liquid volume.

The relationship between electrolyte conductivity and bubble rate is

$$\kappa = \kappa_0(1-\beta)^m\big(1+\lambda(T-T_0)\big), \tag{6}$$

where κ [S/m] is the instantaneous electrolyte conductivity, κ_0 [S/m] is the initial electrolyte conductivity, m is the influence coefficient of bubble rate on conductivity (usually $m = 1.5$), λ is the temperature correlation gradient, T [K] is the instantaneous electrolyte temperature, and T_0 [K] is the initial electrolyte temperature.

According to Ohm's law, the expression for the current density in the MG is

$$i = \frac{U\kappa}{\Delta} = \kappa\nabla\varphi, \tag{7}$$

where i [A/cm^2] is the current density, U [V] is the processing voltage, and Δ [mm] is the MG between the cathode and anode.

During ECM, the chemical reaction at the cathode is

$$2H^{+} + 2e \rightarrow H_2 \uparrow \tag{8}$$

Compared with the amount of hydrogen generated after the chemical reaction, the amount of oxygen precipitated from the anode is negligible. According to Faraday's law, the amount of hydrogen released from the cathode surface can be expressed as [17]

$$N_{H_2} = \frac{i}{2F}, \tag{9}$$

where $F \approx 96\,500$ (A·s/mol, C/mol) is the Faraday constant.

ECM involves both solid and fluid heat transfer; solid heat transfer refers to the heat conduction due to the internal temperatures of the anode and cathode, while fluid heat transfer refers to the heat conduction due to the temperature of the electrolyte [18]. The equation governing the temperature distribution in the MG is

$$\rho C_p\left(\frac{\partial T}{\partial t} + u \cdot \nabla T\right) = \nabla(k\nabla T) + \frac{i^2}{\kappa}, \tag{10}$$

where C_p [J/(kg·°C)] is the specific heat capacity and k is the heat-transfer coefficient.
The heat-transfer boundary conditions are

$$T|\Gamma_{10} = T_0, \tag{11}$$

$$\left.\frac{\partial T}{\partial n}\right| \Gamma_{3,5,9,11} = 0, \tag{12}$$

and the relevant boundary conditions for the moving mesh are

$$v|\Gamma_{6,7,8} = v \tag{13}$$

$$v|\Gamma_{1,2,12} = \eta\omega i \tag{14}$$

where v [mm/min] is the feed rate of the cathode, η is the current efficiency, and ω [mm^3/(A·min)] is the volume electrochemical equivalent.

3.2 Description of cathode vibration

To facilitate the study of VPECM, the cathode motion is generally simplified as harmonic motion, the displacement of which can be described by

$$Y(t) = A\sin(2\pi f t + \varphi), \tag{15}$$

where A [mm] is the vibration amplitude, t [s] is the processing time, f [Hz] is the vibration frequency, and φ is the phase angle. The vibration speed is given by [19]

$$v(t) = \dot{Y}(t) = 2A\pi f\cos(2\pi f t + \varphi). \tag{16}$$

The temporal variations of the vibration displacement and speed of the cathode in a single vibration cycle are shown in Figure 3.

In traditional ECM, the cathode usually moves at a constant feed rate, and when the latter is equal to the dissolution rate of the anode, the processing reaches equilibrium [2]. VPECM also uses a constant feed rate while applying vibration to the cathode, so the feed rate of the cathode is the superposition of its constant feed rate and vibration speed, which is determined by

$$v_m(t) = v_c + v(t) = v_c + 2A\pi f \cos(2\pi f t + \theta), \tag{17}$$

where v_c is the constant feed rate of the cathode.

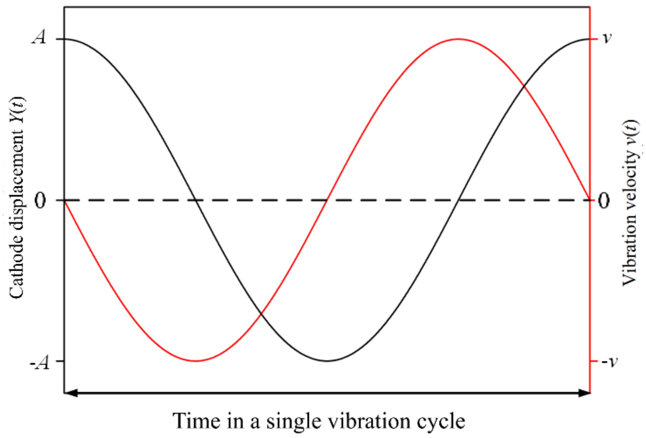

Figure 3. Variations of cathode displacement (black) and speed (red) with time

3.3 Parameter values used in simulations

Table 1 lists the values of the basic parameters used in the simulations. For a fair comparison of PECM and VPECM, the PECM pulse frequency and the VPECM vibration frequency were both set to 10 Hz, and the duty cycle was set to 25%; the power was turned on in the 0.025 s (quarter of a cycle) when the workpiece and cathode were the closest to each other, and the amplitude was 0.3 mm. Figure 4 shows the power-on times for DC-ECM, PECM, and VPECM.

Table 1. Values of basic parameters used in simulations

Condition	Value
Voltage	20 V
Electrolyte conductivity	16.1 S/m
Electrolyte inlet pressure	0.6 MPa
Electrolyte outlet pressure	0.1 MPa
Electrolyte temperature	30°C

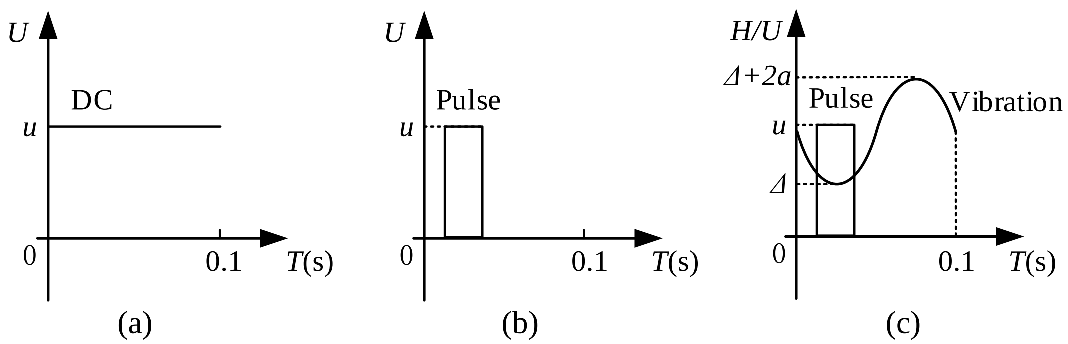

Figure 4. Power-on positions for different types of ECM: (a) DC-ECM; (b) PECM; (c) VPECM

4. ANALYSES USING PHYSICAL MULTI-FIELD-COUPLING SIMULATIONS

4.1 Simulation analysis with machining gap of 0.1 mm

To assess the distribution of products in the machining process, the period of the first vibration cycle (0–0.1 s) was simulated. During this period, DC-ECM is powered on continuously, whereas PECM and VPECM are powered on from 0.0125 s to 0.0375 s; therefore, the three times of 0.015 s, 0.025 s, and 0.035 s were selected. We analyze how the bubble rate and electrolyte temperature and flow rate vary along the processing direction at those three times, as well as how those three quantities vary with time at the inlet, middle, and outlet positions of the process with an MG of 0.1 mm.

Because of the continuous energization of DC-ECM, the distribution of products in its MG tends to be stable with the machining [2]. Figure 5 shows how the bubble rate changes in the DC-ECM MG. Figure 5(a) shows the change of the bubble rate along the processing direction at the three selected times of 0.015 s, 0.025 s, and 0.035 s. As can be seen, the distribution trend of the bubble rate along the processing direction at the three times is consistent, i.e., it accumulates gradually along the flow path, being lowest at the inlet position and highest at the outlet position. Figure 5(b) shows the distribution of the bubble rate in the MG from the inlet position to the outlet position. The bubble rate at the inlet position is stable at ~30% after power-on, that at the middle position is ~78%, and that at the outlet position is ~90%; under such high bubble rates, the processing is very prone to accidents such as short circuits. Therefore, with DC-ECM, it is difficult to maintain machining stability with an MG of 0.1 mm.

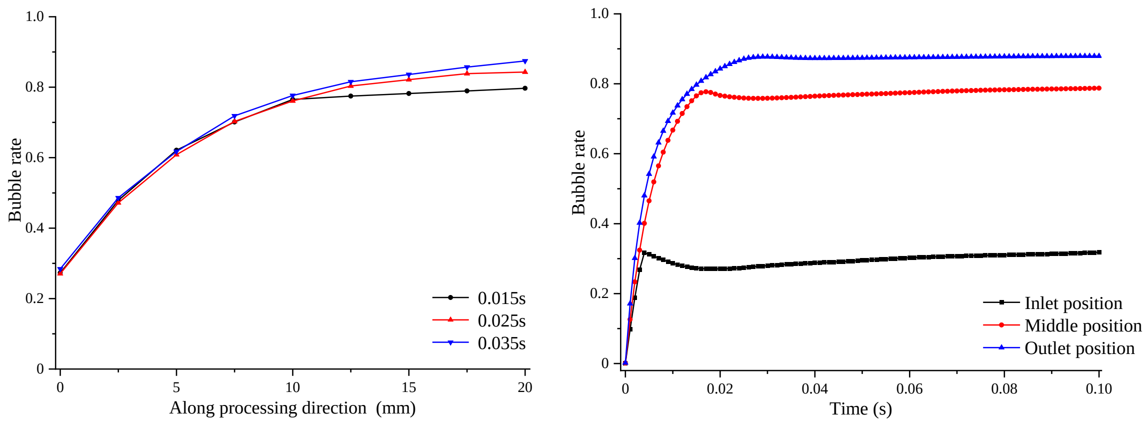

(a) (b)

Figure 5. Changes of bubble rate in DC-ECM (a) along processing direction and (b) at different positions.

Figure 6(a) shows the distribution of the bubble rate along the processing directions at the three selected times in PECM. At 0.015 s, the bubble rate along the processing direction in the MG is low, as is the growth rate, increasing gradually from 20% to 31%. At 0.025 s and 0.035 s, with increasing processing time, bubbles accumulate seriously along the processing direction, reaching 75.3% and 85.4%, respectively, at the final position of the process.

As shown in Figure 6(b), the bubble rates at the inlet, middle, and outlet positions change with time. After PECM starts power-on processing at 0.0125 s, the bubble rates at the three positions increase continuously initially and then decrease. Because of the low degree of bubble accumulation at the inlet position, the bubble rate there is significantly lower than those at the middle and outlet positions; the maximum bubble rate at the outlet is 86.9%. When the power is off at 0.0375 s, more bubbles remain in the gap and are not discharged. The bubble rate at the inlet is low, and the bubbles there are discharged completely at 0.044 s; the time from power-off to complete discharge is 65 ms. The bubble rates at the middle and outlet are relatively high; the bubble rate at the outlet is the highest, with complete discharge by 0.071 s, and the time from power-off to complete bubble discharge is 335 ms.

Compared with DC-ECM, the bubble rate at the inlet position after PECM is powered on is reduced significantly. During the pulse interval, the bubbles are quickly discharged from the MG because of the high-speed scouring of electrolyte, and the bubble rate returns to zero; this will greatly improve the stability of ECM and is expected to give stable processing in this gap state.

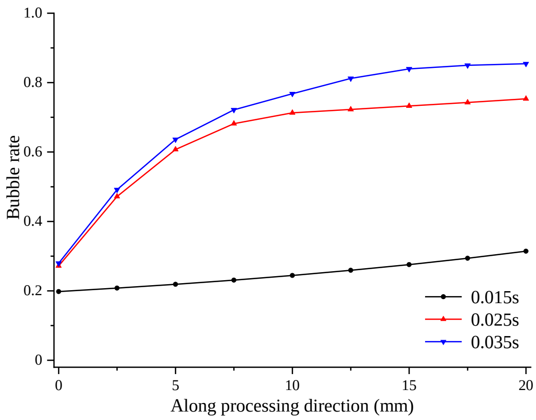

(a)

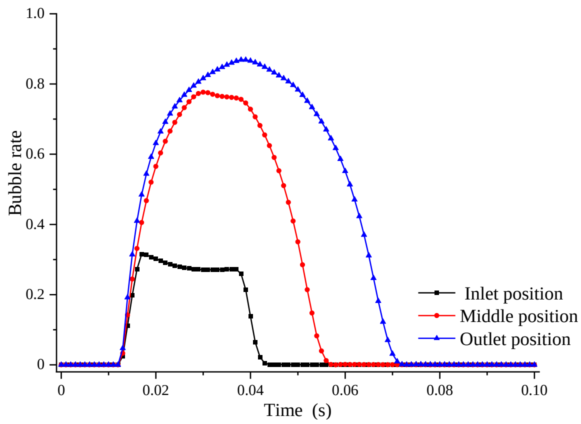

(b)

Figure 6. Changes of bubble rate in PECM (a) along processing direction and (b) at different positions

Figure 7 shows the changes in the bubble rate in the MG during VPECM. Figure 7(a) shows that the highest bubble rate along the processing direction is lower than 14% at 0.015 s, and the growth rate of the bubble rate at each of the three times is lower than those for DC-ECM and PECM, even though the highest bubble rate at the end of the process is lower than 80% at 0.035 s. Figure 7(b) shows the temporal variation of the bubble rate at the different positions. After power-on, as the cathode approaches the workpiece, the bubble rate in the gap rises rapidly. The maximum bubble rate at the outlet is 80.9% at 0.039 s, which is lower than those for DC-ECM and PECM. Similar to PECM, many bubbles remain in the MG after power-off at 0.0375 s. By 0.059 s at the outlet position, the bubbles have been discharged completely. The time from power-off to complete bubble discharge is 215 ms, and the bubble discharge rate is significantly better than that of PECM at the same position.

As can be seen, with an MG of 0.1 mm, the changes of the bubble rate show that the bubble rate of VPECM is the lowest in a power-on cycle, and the time for bubbles to discharge completely from the MG is shorter than that for PECM.

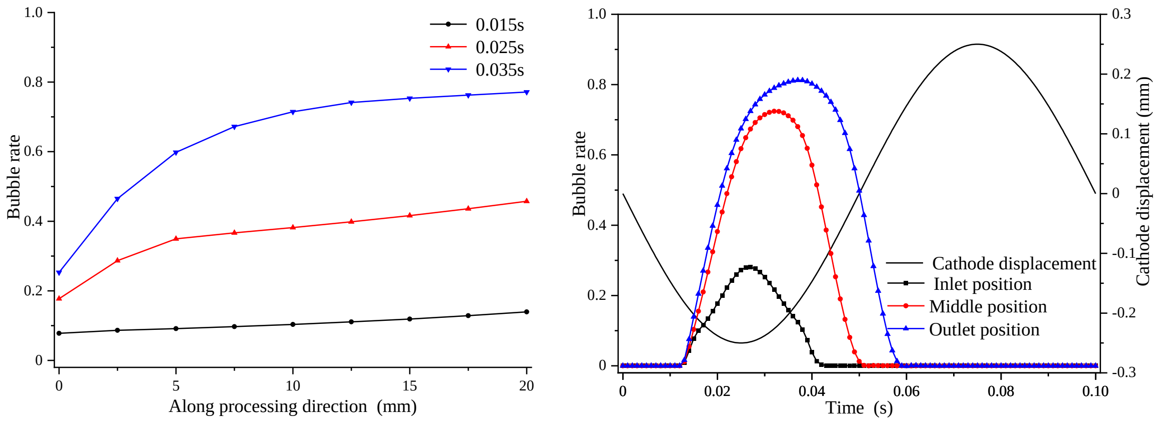

(a) (b)

Figure 7. Changes of bubble rate in VPECM (a) along processing direction and (b) at different positions

Figures 8–10 show the rises in electrolyte temperature for the different types of ECM. The electrolyte temperature increases initially then decreases along the flow direction at 0.015 s, and it increases gradually along the flow direction at 0.025 s and 0.035 s. The electrolyte temperature in PECM and VPECM is low at 0.015 s and increases initially and then decreases at 0.025 s and 0.035 s. From analyzing the changes in electrolyte temperature at the inlet, middle, and outlet positions, the electrolyte temperature continues to rise during DC-ECM, whereas those in PECM and VPECM increase initially and then decrease; the electrolyte temperature in PECM and VPECM is still relatively high when the power is off for 0.0375 s. At the outlet, it takes 335 ms for the Joule heat of PECM to be discharged completely, whereas it takes only 245 ms for VPECM.

As can be seen, intermittent power-on machining is conducive for discharging Joule heat, and the temperature fluctuation of the electrolyte is small, which is conducive for stable electrolyte conductivity, thereby ensuring the accuracy of ECM. Also, the overall temperature of VPECM is lower than that of PECM, and the time for the electrolyte in VPECM to recover its initial temperature is shorter after power-off.

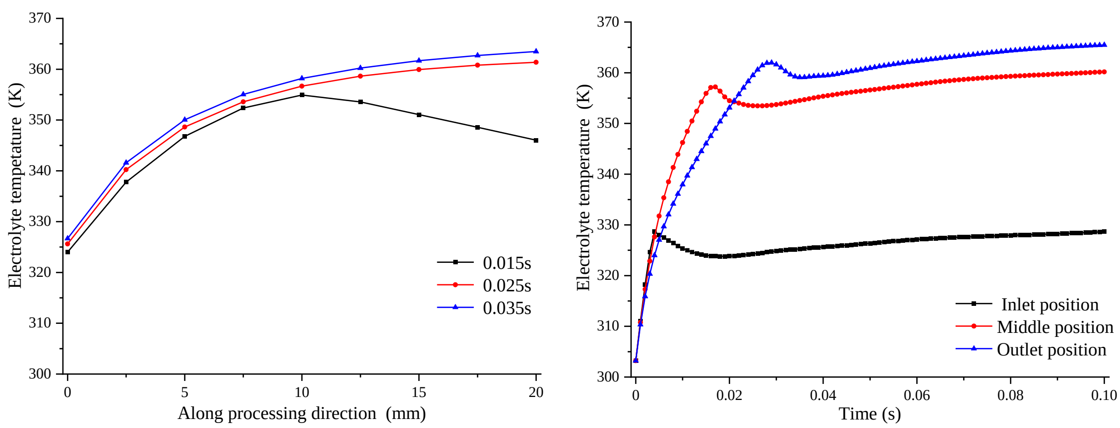

(a) (b)

Figure 8. Changes of electrolyte temperature in DC-ECM (a) along processing direction and (b) at different positions

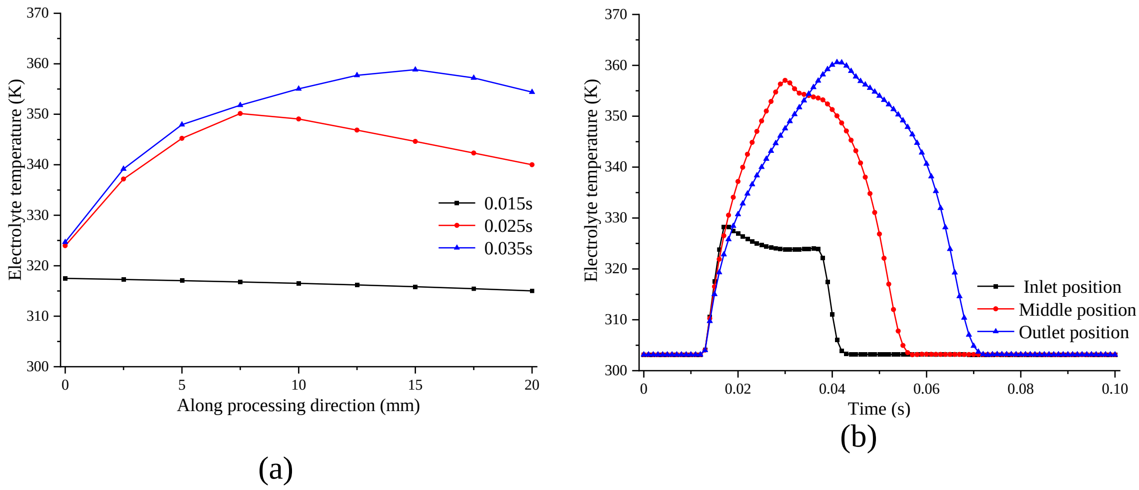

Figure 9. Changes of electrolyte temperature in PECM (a) along processing direction and (b) at different positions

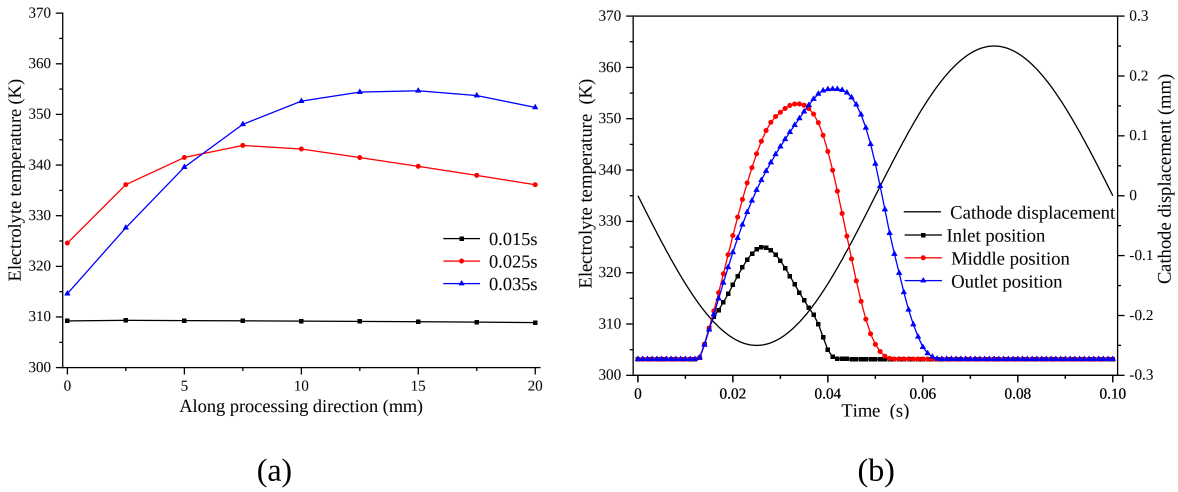

Figure 10. Changes of electrolyte temperature in VPECM (a) along processing direction and (b) at different positions

Figures 11 and 12 show the electrolyte flow rates for the different types of ECM. As can be seen, the variation trends of the electrolyte flow rate at different positions under the three machining methods are the same. Because of the influence of products and Joule heat, the electrolyte flow rate in DC-ECM increases initially and then decreases. This low flow rate is insufficient for removing the products and Joule heat in time, which leads to an extremely unstable machining process and can easily produce short-circuit ablation [20]. Because of the many bubbles generated during processing, PECM has a growth effect on the electrolyte: the electrolyte flow rate has an upward trend after power-on, with a maximum growth rate of 2.5 m/s, which has a positive impact on electrolyte renewal and product discharge. Because of the periodic change of the MG, the electrolyte flow rate shows the same change trend affected by the MG: when the MG becomes smaller, the flow rate decreases, and the minimum flow rate is ~9 m/s; when the cathode retracts and the MG becomes larger, the flow rate increases rapidly, and the maximum flow rate is 19.2 m/s. Therefore, from the perspective of electrolyte flow rate, VPECM is obviously better than DC-ECM and PECM.

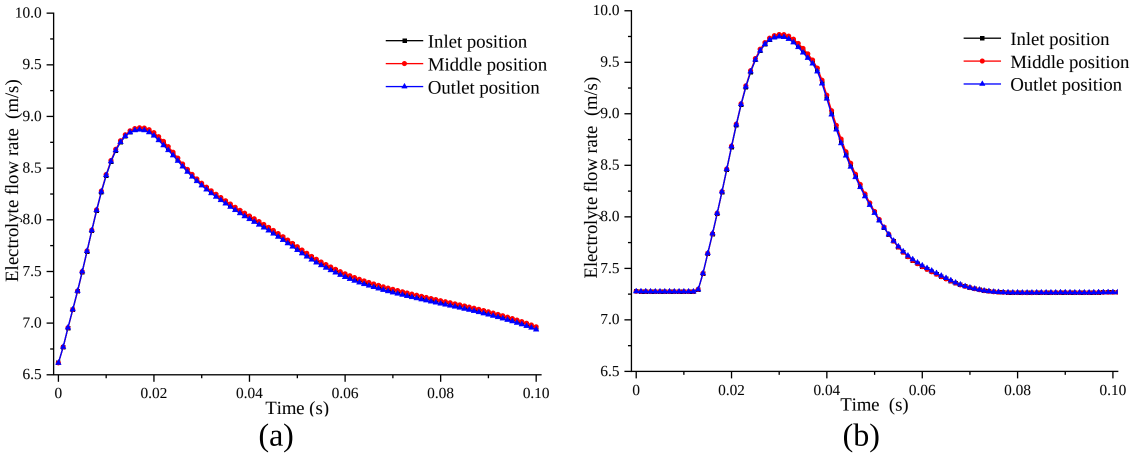

Figure 11. Change of electrolyte flow rate in (a) DC-ECM and (b) PECM

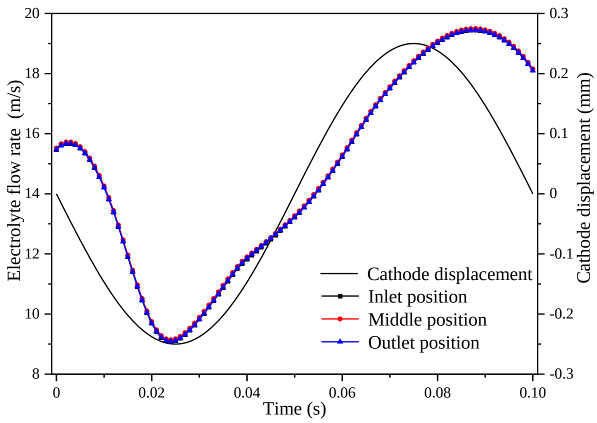

Figure 12. Change of electrolyte flow rate in VPECM

The simulation results show that when the MG is 0.1 mm, the intermittent energization of PECM and VPECM reduce the accumulation of products in the MG, remove the products and Joule heat in time, update the electrolyte and improve the machining stability, especially in VPECM. This result is agreed with the report by Wang et al. [21], which improved machining stability and uniformity through VPECM. Because of the periodic change of the MG, the accumulation of products is less, the temperature rise is low, and the electrolyte flow rate changes periodically: the electrolyte flow rate is high in the large gap, which can accelerate the discharge of products. Therefore, VPECM has significant advantages over DC-ECM and PECM in discharging products and renewing electrolyte in time.

4.2 Simulation analysis with machining gap of 0.01 mm

With the minimum MG of 0.01 mm, we analyze how the bubble rate and electrolyte flow rate change in the different types of ECM at different positions in the process for machining times of 0–0.4 s.

Figures 13 and 14 show the bubble rate and electrolyte flow rate of DC-ECM and PECM in the 0.01-mm MG. We sample and analyze four vibration cycles, and Figure 13(a) shows that the bubble rate of DC-ECM rises rapidly after power-on: it exceeds 90% at the moment of power-on and then approaches 100% rapidly, so the ECM process cannot proceed as normal. Figure 14(a) shows that because of the many bubbles and their rapid generation, especially at the outlet, they cannot be discharged completely during the power-on interval. In the third and fourth cycles, the bubble rate is stable at ~90% and is reduced by only 7% during power-on. From how the electrolyte flow rate changes in Figures 13(b) and 14(b), that of DC-ECM decreases rapidly to zero after power-on, while that of PECM is less than 1 m/s at power-on time. As can be seen, when the MG is 0.01 mm, DC-ECM cannot be carried out because the bubble rate is too high and the flow rate is too low, nor can PECM be carried out because products cannot be discharged during the machining interval.

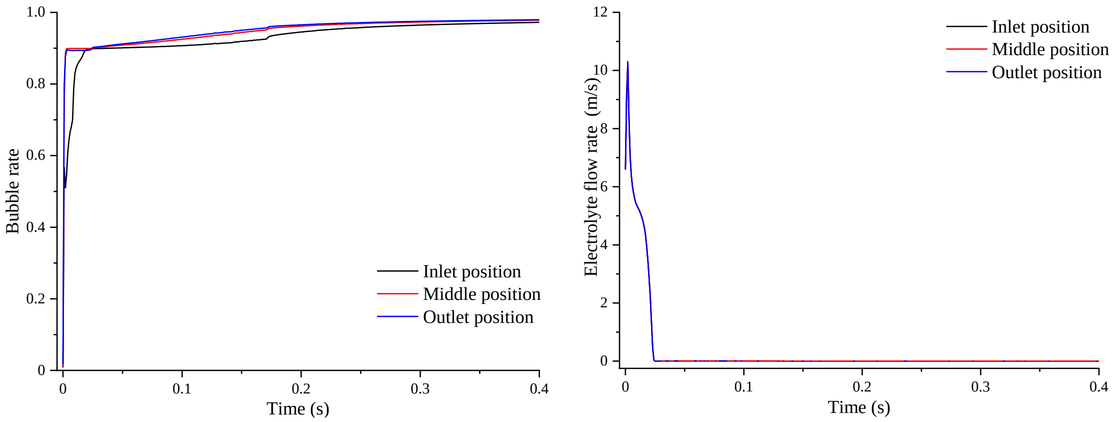

(a) (b)

Figure 13. Changes of (a) bubble rate and (b) electrolyte flow rate in DC-ECM

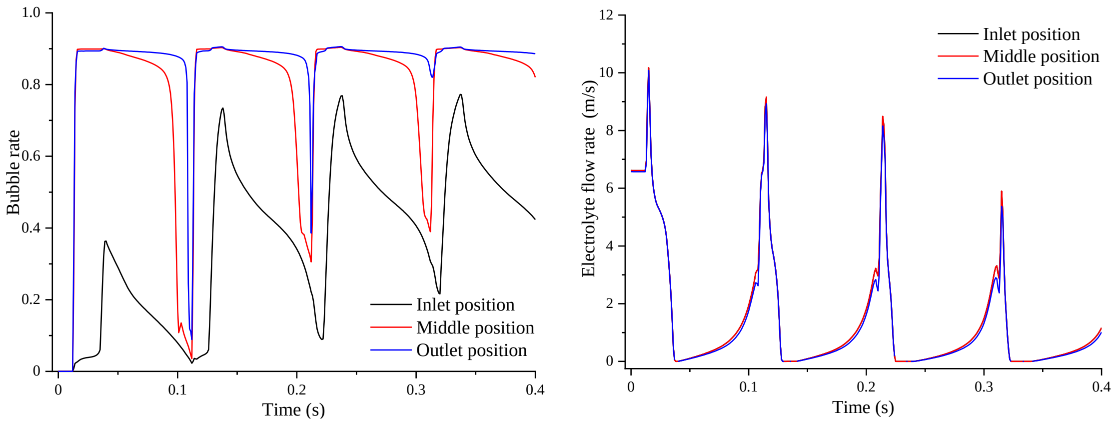

(a) (b)

Figure 14. Changes of (a) bubble rate and (b) electrolyte flow rate in PECM

We also analyze the bubble rate and electrolyte flow rate of VPECM. Figure 15 shows that although the bubble rate is high when the outlet corresponds to the minimum MG, the bubbles in the MG can still be cleared completely after one power-on cycle. Also, the minimum electrolyte flow rate of VPECM is 6 m/s at the minimum MG, and the maximum is 15.8 m/s when the workpiece and cathode are far apart; this will help to discharge products in time and ensure smooth ECM progress.

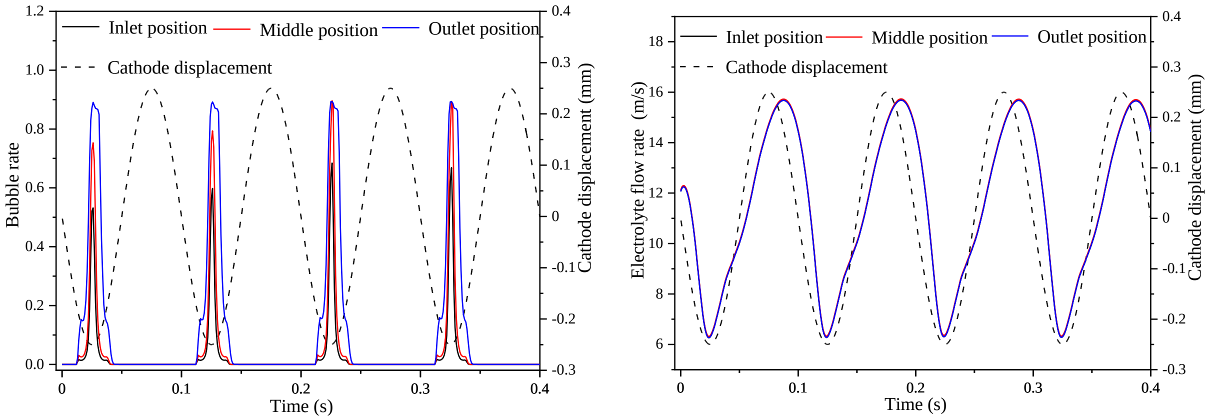

(a) (b)

Figure 15. Changes of (a) bubble rate and (b) electrolyte flow rate in VPECM

In summary, when the MG is 0.1 mm, at the outlet of the process, VPECM has lower bubble rate, lower machining temperature, and higher electrolyte flow rate compared to DC-ECM and PECM, and under the very small MG of 0.01 mm, VPECM can still discharge products in time. Therefore, it is shown clearly that VPECM is advantageous regarding product discharge, can carry out ECM under a smaller MG, and is effective for improving machining accuracy.

5. OBSERVATION AND ANALYSIS OF PRODUCTS WITH HIGH-SPEED CAMERA

From the multi-field-coupling simulations, the differences among DC-ECM, PECM, and VPECM were analyzed, and the advantages of VPECM in product transportation and electrolyte renewal were verified. In this section, we report the results of high-speed camera observations. By observing the products in the MG and recording the corresponding current waveform, we can show the aforementioned differences intuitively.

Figure 16 shows the high-speed camera observation system, the main parts of which were a clamp, a cathode, a light source, and a high-speed camera; also, a storage recorder was used to collect the current and vibration signals of the cathode in the machining process. To enable the tests to be carried out under normal electrolyte pressure, certain changes were made to the experimental setup: the epoxy resin on the front and rear sides of the workpiece and at the cathode processing position shown in the video clip was removed, and transparent tempered glass was used for liquid sealing, thereby facilitating lighting by the light source and shooting by the high-speed camera. The size of the machinable surface of the workpiece and the cathode surface of the fixture was 30 mm × 2 mm, and the values of the basic parameters of the high-speed camera and the ECM are given in Table 2. As in the simulations, for a fair comparison of PECM and VPECM, the PECM pulse frequency and the VPECM vibration frequency were both set to 10 Hz, and the duty cycle was set to 25%; the power was turned on in the 0.025 s (quarter of a cycle) when the workpiece and cathode were the closest to each other (i.e., the power-on processing time in a single power-on cycle was 0.0375–0.0625 s), and the amplitude was 0.3 mm.

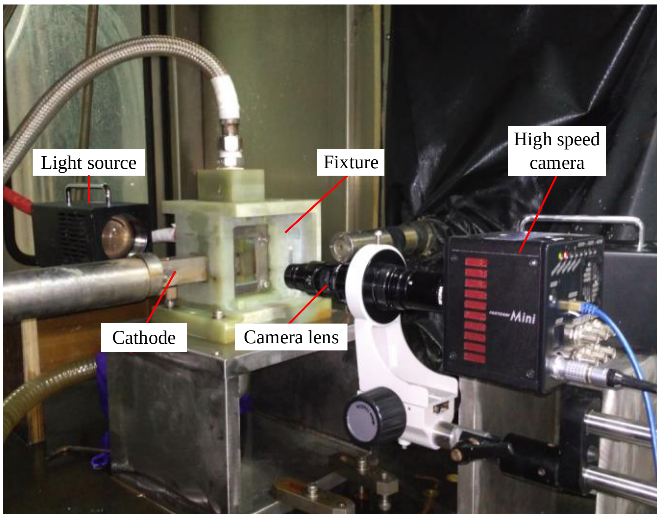

Figure 16. Observation system with high-speed camera

Table 2. Values of basic parameters of high-speed camera and ECM

Condition	**Value**
Camera model	FASTCAM Mini AX200
Camera resolution	512×368
Frame rate	30 000 fps
Electrolyte	20% $NaNO_3$
Voltage	20 V
Electrolyte inlet pressure	0.6 MPa
Electrolyte outlet pressure	0.1 MPa
Electrolyte temperature	30±1°C

Figure 17 shows the results of the high-speed camera observations. The scene was illuminated from the rear, so the brighter parts in the images correspond to clear electrolyte; because of how they affected the light transmittance, bubbles and anode-dissolved products generated by chemical reaction during processing appear as gray and black in the images. Figure 17 shows the observations made for the different types of ECM. During DC-ECM, the MG was always filled with bubbles during the whole machining process; the two pictures shown in Figure 17(a) are typical of all those taken during the machining process. For PECM, the seven pictures shown in Figure 17(b) are divided into six equal parts of quarter power-on cycles in a pulse cycle, and seven pictures (seven discontinuous frames) were taken at seven times; as can be seen, products began to be generated after power-on and the area of light transmission decreased gradually, then the products decreased gradually after power-off and the area of light transmission recovered and expanded. For VPECM in Figure 17(c), quarter power-on cycles during vibration are divided into six equal parts, and seven pictures (seven discontinuous frames) were taken at seven times to see the size change of the MG and the generation of products; frame 7 shows that there were still products in the MG when the VPECM power was cut off.

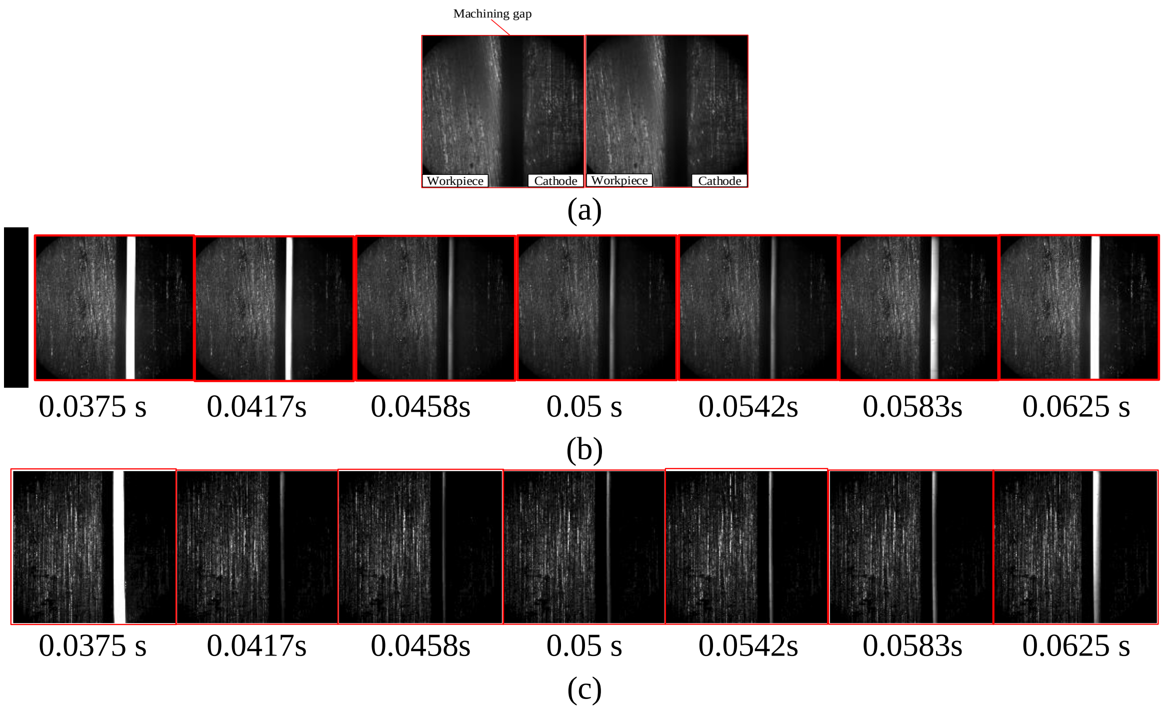

Figure 17. Observation photographs taken using different types of ECM: (a) DC-ECM; (b) PECM; (c) VPECM

Images were selected for seven different power-on times, and image-processing software was used to analyze the gray levels of products for PECM and VPECM. To represent the amount of products, we use the ratio of product layer thickness to MG; a larger ratio represents a higher content of bubbles and anode-dissolved products in the MG, and Figure 18 shows how the ratio changed with time. For VPECM, the bubble rate increased initially and then decreased: at the beginning of power-on, the bubble rate was low, then with the reduction of the MG, it increased gradually, rose to its highest value, and then decreased. However, the thickness of the layer of processed products after the minimum gap was higher than before, which was due mainly to the compression and expansion of the electrolyte during the reciprocating movement with the cathode. For PECM, the bubble rate was generally high at ~57%.

When using the high-speed camera to observe the thickness of the product layer, we also recorded the current density under the different types of ECM. The processing area was 0.6 cm^2, and Figure 19 shows how the current density changed in a single cycle. As can be seen, the current density of DC-ECM was basically unchanged, fluctuating around 25 A/cm^2. When PECM was powered on, its current density had a slight downward trend. For VPECM, the current density increased initially and then decreased, and the peak current density appeared before the minimum MG. VPECM had the highest current density, followed by PECM and then DC-ECM; this shows that in a small MG, DC-ECM cannot reduce the bubble rate and the accumulation of products in a timely and effective manner because of the continuous energization in the machining process, resulting in decreased conductivity and low current density in the MG. In PECM, the conductivity is high because of the intermittent power-on and the rapid scouring of the electrolyte, so the current density when the power is on is higher than that in DC-ECM. VPECM is also intermittent machining, but the current density is the highest because of the disturbance of the cathode reciprocating motion to the electrolyte and the high-speed scouring of the electrolyte in the large MG.

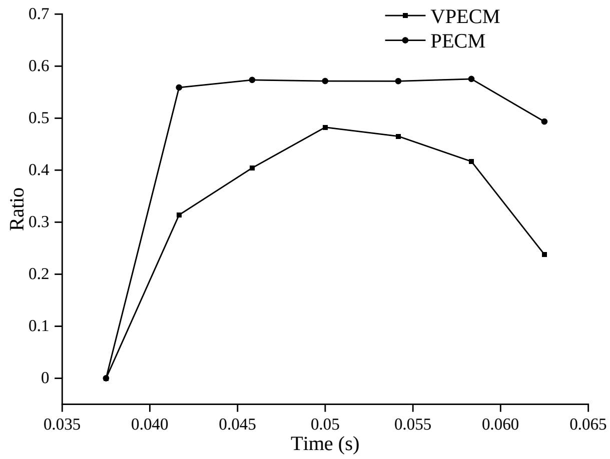

Figure 18. Ratio of measured product layer thickness to machining gap

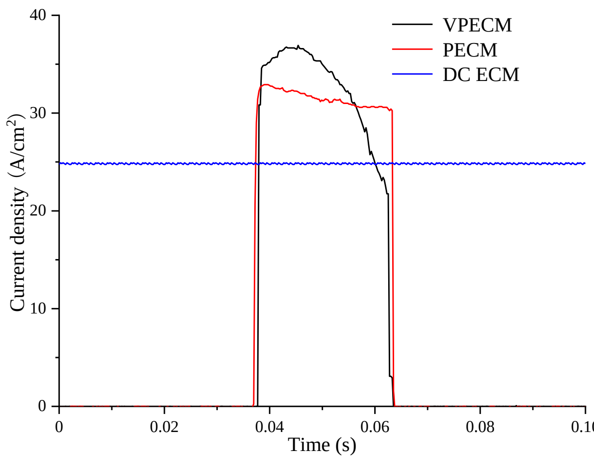

Figure 19. Current density for different types of ECM

5. CONCLUSION

In this paper, through physical multi-field-coupling simulations of DC-ECM, PECM, and VPECM, the product transportation process of ECM was revealed, and the changes of bubble rate, Joule heat, and electrolyte flow rate under different machining methods were analyzed. The results show that under an MG of 0.1 mm, VPECM can discharge bubbles and Joule heat in the MG in a shorter time and has a higher electrolyte flow rate. At a very small MG of 0.01 mm, DC-ECM and PECM have high bubble rate and low flow rate, which cannot be processed in actual machining. However, VPECM can still discharge bubbles in each vibration cycle, and the flow rate of electrolyte is high, which has obvious machining advantages. Through high-speed camera observations, the thickness of the bubble layer in the MG for the different types of ECM was observed, analyzed, and compared, and combined with the current density in the machining process, the machining advantages of the VPECM method were verified.

ACKNOWLEDGEMENTS
This article was sponsored by the Doctoral research funds of Shandong Jianzhu University (X20057Z0101).

References

1. A. Kumar and B. S. Pabla, *Mater. Today: Proc.,* 46 (2021) 10854.
2. Z. Y. Xu and Y. D. Wang, *Chinses J Aeronaut.*, 34 (2019) 28.
3. F. Z. Han, W. Chen, W. C. Ying and J. Zhang, *Procedia CIRP*, 68 (2018) 493.
4. X. L. Fang, X. H. Zou, P. F. Zhang, Y. B. Zeng and N. S. Qu, *Int J Adv Manuf Tech.*, 84 (2016) 929.
5. N. S. Qu and Z. Y. Xu, *Int J Adv Manuf Tech.*, 68 (2013) 1565.
6. Y. Liu, J. Liu, D. Zhu and H Wang, *Chinses J Aeronaut.*, 35 (2022) 461.
7. H El-Hofy, *Int J Adv Manuf Tech.*, 105 (2019) 579.
8. E. S. Lee, S. Y. Baek and C. R.Cho, *Int J Adv Manuf Tech.*, 31 (2007) 762.
9. Z. Brusilovski, *J Mater Process Tech.*, 196 (2008) 311.
10. S. V. Damme, G. Nelissen and B. V. D. Bossche, *J Appl Electrochem.*, 36 (2006) 1.
11. M. S. Hewidy, S. J. Ebeid, T. A. El-Taweel and A. H. Youssef, *J Mater Process Tech.*, 189 (2007) 466.
12. B. Bhattacharyya, M. Malapati, J. Munda and A. Sarkar, *Int J Mach Tool Manu.*, 47 (2007) 335.
13. B. Ghoshal and B. Bhattacharyya, *Int J Mach Tool Manu.*, 64 (2013) 49.
14. A. Ruszaj, S. Skoczypiec, J. Czekaj, T. Miller and J. Dziedzic, *15th International Symposium on Electromachining*, (2007) 309.
15. F. Wang; J. S. Zhao, X. L. Zhang, Z. W. Yang, W. M. Gan, and Z. J. Tian, *Int J Adv Manuf Tech.*, 90 (2017) 971.
16. X. L. Fang, N. S. Qu, Y. D. Zhang, Z. Y. Xu and D. Zhu, *J Mater Process Tech.*, 214 (2014) 556.
17. R. V. Tijum and P. T. Pajak, *Am J Phys Med Rehab.*, 84 (2012) 287.
18. Y. L. Chen, X. C. Zhou, P. X Chen and Z. Q. Wang, *Chinses J Aeronaut.*, 33 (2020) 1057.
19. X. C. Jiang, J. Liu, D. Zhu, M. M. Wang and N. S. Qu, *Appl. Sci.-Basel*, 8 (2018).
20. J. Liu, Y. Liu, X. C. Jiang and D. Zhu, *Int J Adv Manuf Tech.*, 116 (2021) 2031.
21. F. Wang; J. S. Zhao, D. M. Liu, Y. T Fan and Z. J. Tian, *Int. J. Electrochem. Sci.*, 13 (2018) 9466.